Ultra-low cost and energy-efficient production of FePCSi amorphous alloys with pretreated molten iron from a blast furnace

Guoyang Zhang[a,b,c], Hua Zhang[a,b,*], Shiqiang Yue[a,b], Anding Wang[c,d,**], Aina He[c], Rijin Cheng[a,b], Yaqiang Dong[c], Hongwei Ni[a,b], Chain-Tsuan Liu[d]

[a] *The state key laboratory of refractories and metallurgy, Wuhan University of Science and Technology, Wuhan 430081, China*
[b] *Key laboratory for ferrous metallurgy and resources utilization of ministry education, Wuhan University of Science and Technology, Wuhan 430081, China*
[c] *CAS Key Laboratory of Magnetic Materials and Devices, Zhejiang Province Key Laboratory of Magnetic Materials and Application Technology, Ningbo Institute of Materials Technology and Engineering, Chinese Academy of Sciences, Ningbo, Zhejiang 315201, China*
[d] *Department of Materials Science and Engineering, City University of Hong Kong, Tat Chee Avenue, Kowloon Tong, Kowloon, Hong Kong, China*

A B S T R A C T

Due to the high sensitivity of amorphous forming ability on purity, Fe-based amorphous alloys are always made with high-purity raw materials which are energy wasting for purification and expensive, thereby limiting their wider application. Here, we proposed an ultra-low cost and energy-efficient production process for Fe-based amorphous alloys, with pretreated molten iron from the blast furnace. $Fe_x(P_{10}C_9Si_1)_{5-0.05x}$ ($x = 76$–82) amorphous alloys with excellent manufacturability and magnetic properties were successfully prepared with the new process. The impurities containing C, P, and Si in the molten iron from a blast furnace were used as useful components, while other minor impurities like Ti and Mn do not apparently affect the GFA and magnetic properties. Attractive magnetic properties, including low H_c of 3.1–5.1 A/m, high μ_e of 6.1–8.4 $\times 10^3$ at 1 kHz, high B_s of 1.25–1.48 T were achieved in ribbon samples after optimal annealing. Rod samples with a diameter up to 1.5 mm were readily prepared and exhibit high strength of 3.37 GPa. The ultra-low cost, energy saving effects and excellent soft magnetic properties will render the production process a new generation for Fe-based amorphous alloys and widen the applications.

1. Introduction

Fe-based amorphous alloys are most attractive among the amorphous alloy community due to their exceptional soft magnetic properties, high strength, high hardness, superb thermal stability, high-efficient degradation and low cost [1]. Therefore, great efforts have been devoted to developing more and more alloy systems, understanding the structure-properties connection mechanisms and generalizing the applications [2–5]. It is generally recognized that the amorphous alloys exhibit a large composition range for high amorphous forming ability (AFA) [6], yet are extremely sensitive to the purity of the raw materials [7–10]. Among the diverse interpretations for the impurity effect, the most credible and acceptable statement is from the heterogeneous nucleation sites for stimulating the crystallization [11]. The impurity-induced substantial decrease of AFA and manufacturability has become a long-standing dilemma for the application of almost all structural and functional amorphous alloys [12]. There are generally three routes for evading or overcoming these troubles: 1) using raw materials with high purity without considering the price in the laboratory experiments which is only acceptable for composition exploration [13–15]; 2) purifying the raw materials to remove the impurities which is energy wasting and complicated in processes [12,16]; 3) adapting the composition to the industrial raw materials [9]. The last route is easier said than done, but the most feasible for mass production, requiring more hard works.

In this study, a novel ultra-low-cost and energy-efficient production process with pretreated molten iron from a blast furnace is proposed and FePCSi amorphous alloys which can well accommodate the impurity-rich raw material were developed. As sketched in Fig. 1, we select the C saturated-dissolved molten iron from a blast furnace as Fe and C sources and use the heat for subsequent alloying and melt-spinning processes. Only a conventional pretreatment of hot metal is kept
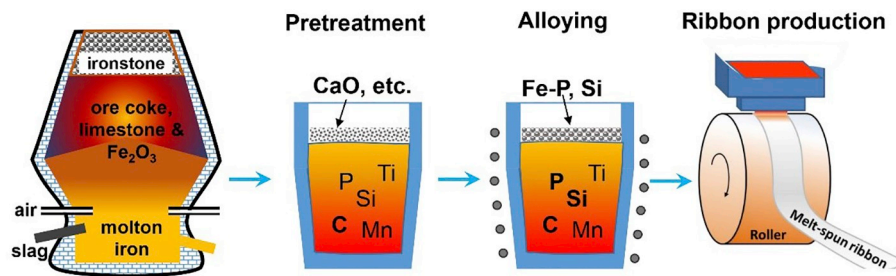
Fig. 1. Sketch of an ultra-low cost and energy-efficient production process of FePCSi amorphous alloys with pretreated molten iron from a blast furnace.

for desulfuration and slagging off. The long metallurgy process of Fe purification is hence substantially shortened and most of the energy is saved. The process is so much simplified idealizedly that the composition exploration is of high difficulties. According to a statistical results of the Fe-based alloys systems, FeSiB [17], FePC [3], FeSiBP [4], Fe-MoPCB [18], FeSiBNb [19], FeBNbY [20] and their micro-alloyed derivative are well reported high AFA systems. Here, only high C content alloys can be selected and metallic elements which will greatly decrease the magnetization should be avoided [21], compelling us to choose Si, P and B which are also cheap and prone to enhance the AFA. After timely adjusting the composition, $Fe_x(P_{10}C_9Si_1)_{5-0.05x}$ ($x = 76–84$) alloys with high impurity tolerance, superb manufacturability and magnetic properties were developed, by referring the documented $Fe_{80}P_{11}C_9$ alloy with high AFA in high purity condition [3]. The AFA, soft magnetic properties, thermal parameters as well as mechanic properties were systemically evaluated. The influence of impurity was studied by comparing with high purity alloys, proving the feasibility of the short process and the potential of the application.

2. Experiment procedures

As we still did small batch experiments, the process in Fig. 1 was not completely used in this study, but simulated to the greatest extent. The industrial raw materials (IRMs) containing pretreated molten iron, industrial Fe-P pre-alloy, pure Fe and Si were taken from Wuhan iron and steel (group) company and the concentrations were listed in Table 1. The pretreated molten iron was taken from the conventional ironmaking line after the desulfuration and slagging off processes. The minor elements containing C, Si, Mn, P, S and Ti were then accurately determined by using a direct reading spectrograph calibrated with reference sample. The Fe, Si, P and C elements in the raw materials are all calculated and used in the composition design process. The total content of the minor elements containing Mn, S, Al and Ti is < 0.1%, which will not induce large composition difference. Multicomponent alloys with nominal atomic compositions of $Fe_x(P_{10}C_9Si_1)_{5-0.05x}$ ($x = 76, 78, 80, 82, 84$) were designed and melt by induction melting under Ar atmosphere after a high vacuum of 10^{-2} Pa in a laboratory. $Fe_{80}P_{10}C_9Si_1$ alloy was also prepared with pure raw materials (PRMs) of Fe (99.99%), Si (99.999%), pre-alloy of Fe_3P and Fe-4.3%C for comparison. The

master alloys were melted by induction melting under high purity argon atmosphere. Ductile amorphous ribbons with high surface quality and width of 1.1–1.2 mm were prepared by single roller melt-spinning technique. Amorphous rods using copper mold casting method under high purity argon and air atmosphere.

Melting and solidification behaviors of the master alloys were tested by differential scanning calorimetry (DSC, NETZSCH 404C) at a heating rate of 0.67 °C/s and low cooling rate of 0.067 °C/s to reduce the effect of undercooling. The thermal parameters of amorphous ribbons were identified by DSC at a heating rate of 0.67 °C/s. According to the thermal parameters, the as-spun ribbons were isothermally annealed at a suitable temperature range for 10 min under high vacuum. The microstructure of samples was investigated by X-ray diffraction (XRD, Bruker D8 Advance) with Cu-Kα radiation and scanning electron microscope (SEM, FEI Quanta FEG 250). More than three samples were tested for H_c, μ_e and B_s data to obtain an average value. The magnetic properties of coercive force (H_c), effective permeability (μ_e) and saturation magnetization (B_s) were evaluated by B-H loop tracer (EXPH-100) under the maximum applied field of 800 A/m, impedance analyzer (Agilent 4294 A) under the applied field from 1 to 100 A/m and vibrating sample magnetometer (VSM, Lake Shore 7410) under the maximum applied field of 800 kA/m, respectively. The magnetic domain structure was characterized via the Magneto-optical Kerr Microscope (MOKE, Evico 4-873 K/950 MT). The compression test was conducted by using cylindrical rods (1 mm in diameter and 2 mm in length) with a universal testing machine (CMT5205 SANS, China) at a strain rate of $5 \times 10^{-4}\,s^{-1}$. All the measurements without special explanation were performed at room temperature.

3. Results

3.1. Thermal properties and amorphous-forming ability

The influences of impurities on melting and solidification processes were firstly investigated, by comparing the $Fe_{80}P_{10}C_9Si_1$ master alloys and ribbons made with PRMs and IRMs. As shown in Fig. 2a, the DSC curves of alloys made of IRMs and PRMs show neglectable difference both in the melting and solidification sections, proving the high impurity tolerance of this alloy system. The offset temperatures (T_{ml}) in

Table 1
Composition and price comparison of raw materials.

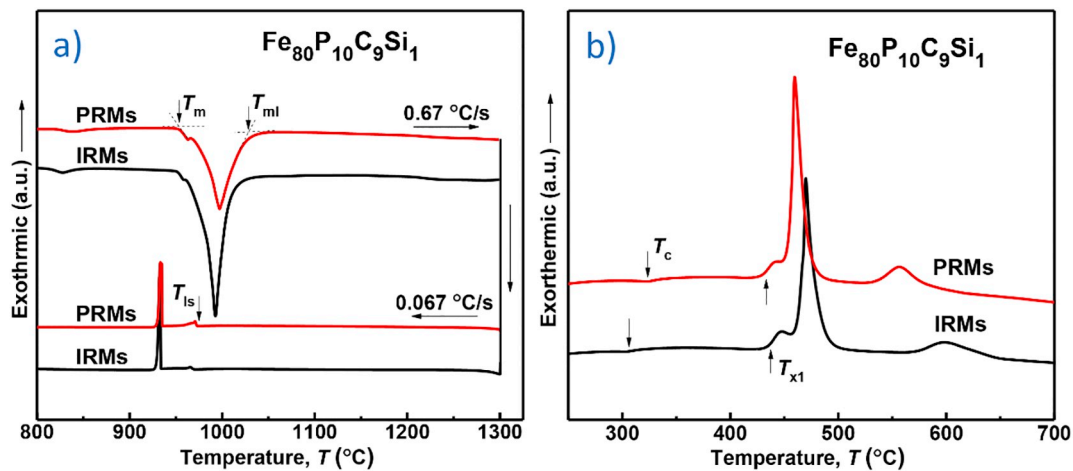| Raw materials		Content of elements (wt%)								Price (¥/kg)
		Fe	P	C	Si	Mn	S	Al	Ti	
IRMs	Molten iron	95.290	0.102	4.097	0.340	0.11	0.001		0.031	2.3
	Fe-P alloy	72.752	26.50	0.098	0.600	0.70	0.050			2.5
	Fe	99.6	0.006	0.002	0.005	0.01	0.005	0.01	0.001	6
	Si	0.27			99.7			0.03		10
PRMs	Pure Fe	99.99								3000
	Fe_3P alloy	15.6	84.4							60,000
	FeC alloy	95.7		4.3						20,000
	Si	99.999								500

Fig. 2. Results of comparative samples prepared with PRMs and IRMs: a) DSC traces of $Fe_{80}P_{10}C_9Si_1$ master alloys showing the melting and solidification processes; b) DSC traces of ribbons showing the crystallization behaviors.

melting process section of the IRMs sample is even lower than that of the PRMs samples. It is noting that both onset temperature (T_m) of melting process and the onset temperature (T_{ls}) of the solidification process exhibit really low values ($< 1000\,°C$) which are much lower than most of the Fe-based alloys with high AFA [19], although the $Fe_{80}P_{10}C_9Si_1$ alloy deviates slightly from the eutectic point. Fig. 2b shows the DSC curves of $Fe_{80}P_{10}C_9Si_1$ amorphous ribbons prepared with PRMs and IRMs. The impurities in IRMs do not apparently affect the crystallization events but slightly changes the temperature. The onset temperature (T_{x1}) of the first crystallization peak of IRMs ribbons is slightly higher than the PRMs, indicating higher stability and resistance of crystallization [22]. The Curie temperature (T_c) of the IRMs ribbons is 11 °C lower, leading to a wider annealing window in the T_c and T_{x1} range. Overall, the verification experiments deliver positive messages that the FePC system alloys exhibit high impurity tolerance and can be adapted to the industrial raw materials and the short production process in Fig. 1.

Then, ribbon and rod samples of $Fe_x(P_{10}C_9Si_1)_{5-0.05x}$ ($x = 76, 78, 80, 82, 84$) alloys were made with IRMs and evaluated systemically. Fig. 3a shows the XRD patterns of the as-quenched ribbons prepared with a wheel speed of 40 m/s with a quite good ductility and surface quality. Except for the one with $x = 84$, all ribbons exhibit typical XRD patterns of amorphous structure, indicating the achievement of the upper limit of Fe content of 84 at. %. The precipitation of α–Fe and Fe_3C phases indicates the poor AFA of the $Fe_{84}(P_{10}C_9Si_1)_{0.8}$ alloy. This result

well supports the feasibility of production of $Fe_x(P_{10}C_9Si_1)_{5-0.05x}$ ($x = 76–82$) amorphous alloys with pretreated molten iron from a blast furnace. To deeper identify the AFA of these alloys made with IRMs, copper mold casting method was employed and rod samples with different diameters were prepared. Fig. 3b shows XRD patterns of samples with critical dimensions. It is exciting that the $Fe_x(P_{10}C_9Si_1)_{5-0.05x}$ ($x = 76, 78, 80, 82$) alloys made with IRMs exhibit high AFA. Rod samples with diameters of 1–1.5 mm were readily pared for the alloys with $x = 76–80$. For the high Fe content $Fe_{82}(P_{10}C_9Si_1)_{0.9}$ alloy, ribbon with a thickness of 43 μm can also be made with a wheel speed of 20 m/ s which are absolutely acceptable for industrial mass production. Compared with the alloys made with PRMs, the $Fe_{80}P_{10}C_9Si_1$ alloy made with IRMs exhibits almost the same AFA, further stressing the high impurity tolerance. It is interesting that the $Fe_{80}P_{10}C_9Si_1$ sample made in air shows a larger critical size than that made in Argon, indicating the enhancement of AFA by Air and good adaptability of mass production in the air [23]. It is hence concluded that the $Fe_x(P_{10}C_9Si_1)_{5-0.05x}$ ($x = 76, 78, 80, 82, 84$) alloys exhibiting high impurity tolerance and manufacturability can be made with industrial raw materials and pretreated molten iron from a blast furnace.

The melting and solidification processes of the master alloys, as well as the crystallization behavior of $Fe_x(P_{10}C_9Si_1)_{5-0.05x}$ ($x = 76, 78, 80, 82, 84$) alloys made with IRMs were studied to understand the origin of high AFA and provide a reference for the following annealing. Fig. 4a shows DSC curves of $Fe_x(P_{10}C_9Si_1)_{5-0.05x}$ ($x = 76, 78, 80, 82, 84$)

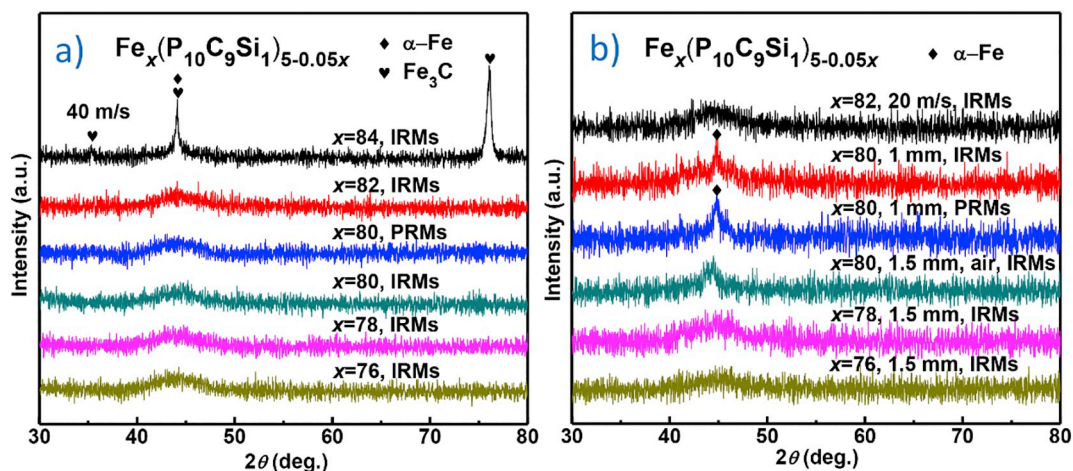**Fig. 3.** XRD patterns of $Fe_x(P_{10}C_9Si_1)_{5-0.05x}$ ($x = 76, 78, 80, 82, 84$) alloys made with IRMs a) the as-spun ribbons alloys prepared with a wheel speed of 40 m/s; b) the as-cast rods and ribbons with critical size. The samples made with PRMs were also shown for comparison.
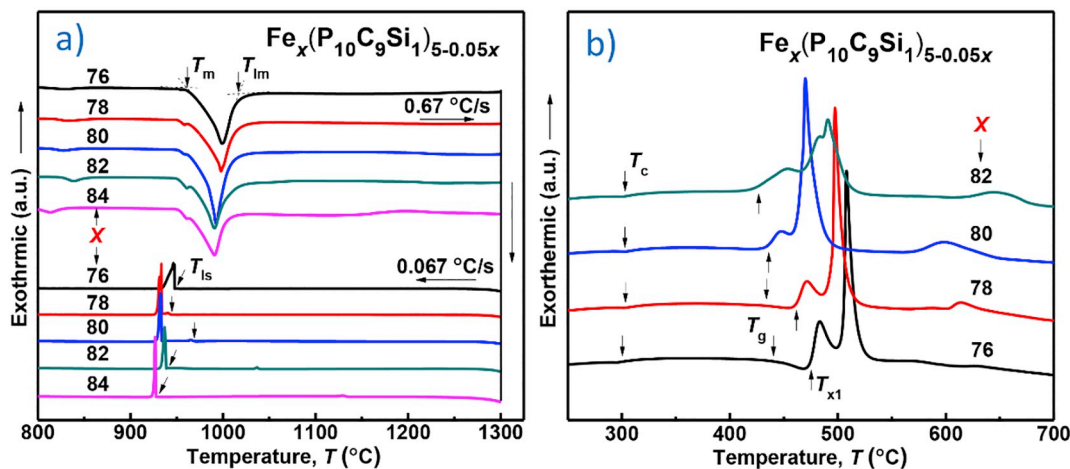
Fig. 4. DSC curves of $Fe_x(P_{10}C_9Si_1)_{5-0.05x}$ (x = 76, 78, 80, 82, 84) alloys prepared with IRMs: a) melting and solidification processes of master alloys; b) crystallization process of amorphous ribbons.

master alloys. With the increase of Fe content, it is unexpectedly that the T_m and T_{lm} decrease slightly, which is quite different with the conventional Fe-based alloys, such as FeSiB [24], FeSiBPC [25], FeSiBNb [19] and etc. This result indicates that the alloys approach the eutectic point of $Fe_x(P_{10}C_9Si_1)_{5-0.05x}$ (x = 76, 78, 80, 82, 84) alloys with the increase of Fe content and may exhibit a high AFA. We can also deduce that the Fe content of the eutectic FePCSi alloys is higher than that of the FeSiB, FeSiBPC and FeSiBNb alloys. In addition, the change of Fe content slightly affect the temperature of the main exothermic peak during the solidification process. The DSC curves of IRMs $Fe_x(P_{10}C_9Si_1)_{5-0.05x}$ (x = 76, 78, 80, 82) as-spun amorphous ribbons are showed in Fig. 4b. It is clear that the increase of Fe content leads to the disappearance of glass transition and a slight decrease of the T_{x1}. The T_c of the alloys shows a weak or no connection with the Fe content, resulting in a large temperature interval of T_{x1} and T_c which is important for achieving superior soft-magnetic properties [26]. The exceptional changes of T_m, T_{lm} and T_c on Fe content are very interesting scientific issues and will render FePCSi system alloys good model materials for the future understanding of the atomic interactions, but are not the focus in this study. According to the commonly used AFA criterions based on the thermal parameters [27], including T_{rg} ($= T_g/T_l$), α ($= T_x/T_l$), ΔT_x ($= T_x - T_g$) and γ ($= T_x/(T_g + T_l)$), the ultra-low T_m, T_{lm} and T_{ls} will be the reason for the high AFA of this alloy system. The decreased T_m, T_{lm} as well as slightly decreased T_{x1} might be the reasons why the IRMs alloys with x = 80 and 82 still keep a high AFA.

3.2. Magnetic properties of amorphous alloy ribbons

After confirming the feasibility of the production process and the high AFA of the $Fe_x(P_{10}C_9Si_1)_{5-0.05x}$ (x = 76, 78, 80, 82) alloys, we investigated the magnetic properties and the influence of impurities for amorphous samples prepared with IRMs. According to the T_c (303 °C) and T_x (434 °C), annealing was conducted in the T_A range of 320–400 °C for 10 min, for internal stress releasing and structure relaxation [28]. Fig. 5a and b exhibit the annealing temperature (T_A) dependences of H_c and μ_e at 1 kHz for $Fe_{80}P_{10}C_9Si_1$ amorphous ribbons prepared with IRMs and PRMs. The variation tendencies of H_c and μ_e for the PRMs and IRMs samples show no difference. Low H_c of about 3.1 A/m can be obtained at 320 °C for the IRMs samples which are even lower than the PRMs samples. Besides, the optimal annealing parameter windows for IRMs and PRMs samples are also absolutely the same. According to the μ_e results, the IRMs samples exhibit high μ_e of about 6.3×10^3 at 1 kHz under 1 A/m. It should be noticed that the maximum μ_e of IRMs is lower than the PRMs, which could be interpreted to the pinning effect of non-magnetic impurities on magnetic domains or other reasons. The

saturated magnetization loops of PRMs and IRMs $Fe_{80}P_{10}C_9Si_1$ alloys annealed optimally at 340 °C for 10 min were measured by VSM, as shown in Fig. 5c. The B_s of IRMs ribbon exhibits a high B_s 1.45 T, which is slightly lower than 1.49 T of the PRMs samples due to the non-magnetic impurities and the composition deviation of raw materials.

Then, we further investigated the magnetic properties of the $Fe_x(P_{10}C_9Si_1)_{5-0.05x}$ (x = 76, 78, 80, 82) alloys prepared with IRMs. As shown in Fig. 6a and b, all alloys with different Fe content achieve the optimal soft magnetic properties, including low H_c of 3.1–5.1 A/m and high μ_e of $6.3–8.4 \times 10^3$, which is comparable with the FeSiB alloys [24]. Unlike the slight variation of T_{x1}-T_c value, the optimal T_A window decreases greatly with the increase of Fe content. According to the hysteresis magnetic loops of annealed ribbons shown in Fig. 6c, the B_s increases gradually from 1.25 T to 1.48 T with the increase of Fe content.

Table 2 gathers the critical diameters, thermal parameters, magnetic properties and oxygen content of $Fe_x(P_{10}C_9Si_1)_{5-0.05x}$ (x = 76, 78, 80, 82) amorphous alloys. The FePCSi alloys made with IRMs exhibit high AFA and attractive magnetic properties, which can be adjusted according to the application requirement. The low T_m and T_{ls} indicate the mild ribbon production process and good manufacturability. The low T_c and a large T_{x1}-T_c window will be propitious to low-temperature annealing which is energy efficient and prone to improve the ductility of ribbons. The alloys with x = 76–80 exhibit high AFA of 1.5 mm and moderate B_s, which are better than the commercial Fe-based amorphous alloy for powder production [29]. The $Fe_{82}(P_{10}C_9Si_1)_{0.9}$ alloy exhibit the highest B_s and comprehensive magnetic properties as well as acceptable AFA for mass ribbon production is a good candidate for substituting the commercial FeSiB alloys.

Since soft-magnetic materials work under different applied magnetic field and frequency, we evaluated the μ_e of $Fe_{82}(P_{10}C_9Si_1)_{0.9}$ alloy ribbons prepared with IRMs more detailedly. As shown in Fig. 7a, the μ_e of the alloy ribbons increases first with the increasing of the magnetic field (H_m) and then maximizes to a superior value of about 23×10^3. Moreover, the μ_e keeps stable in a wide f range of 1–10 kHz which is important for the application. For further understanding the outstanding magnetic properties of this alloy, the magnetic domains of the representative $Fe_{82}(P_{10}C_9Si_1)_{0.9}$ alloy ribbon under optimum annealing were characterized under zero field via the Magneto-optical Kerr Microscopy. As shown in Fig. 7b, wide stripe domains perpendicular to the ribbon direction were detected on the free surface of amorphous ribbons annealed at 340 °C for 10 min. The low pinning effect deduced from the large width and the smooth edge of the domains should be the reason for the outstanding soft magnetic properties. The high amorphicity originated from high AFA and larger T_{x1}-T_c will also lead to
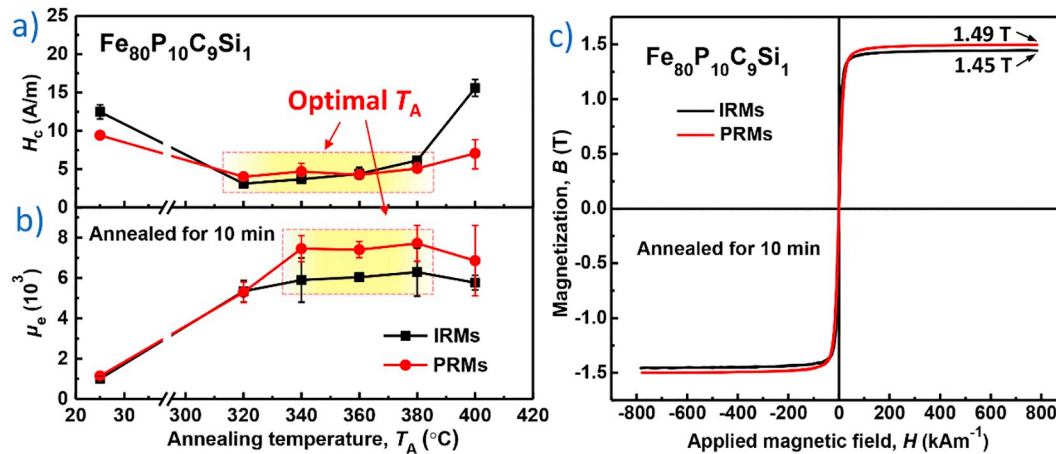
Fig. 5. a-b) T_A dependence of H_c and μ_e at 1 kHz for $Fe_{80}P_{10}C_9Si_1$ alloys ribbon made with PRMs and IRMs; c) saturated magnetization loops of PRMs and IRMs $Fe_{80}P_{10}C_9Si_1$ alloys annealed at 340 °C for 10 min.

uniform microstructure, thorough free volume annihilation and stress release [28], during annealing for structural relaxation.

3.3. Mechanical properties of bulk amorphous samples

By using the low-cost IRMs, $Fe_{78}(P_{10}C_9Si_1)_{1.1}$ and $Fe_{76}(P_{10}C_9Si_1)_{1.2}$ alloys are easy cast into bulk amorphous samples, according to the XRD patterns shown in Fig. 3b. This is also very attractive for application of Fe-based amorphous alloys in devices requiring bulk samples. Therefore, the compression test was taken to evaluate the mechanical properties of the alloys. As shown in Fig. 8a, the compressive stress-strain curves for the rod samples with a diameter of 1 mm show high yield and fracture strength of about 3.25–3.37 MPa which are higher than the 3.22 MPa of the $Fe_{80}P_{11}C_9$ alloy made with PRMs. Compared with the documented plasticity of 1.4% of $Fe_{80}P_{11}C_9$ alloy [3], the plasticity s decrease to about 0.5% for $Fe_{76}(P_{10}C_9Si_1)_{1.2}$ alloy and almost 0% for $Fe_{78}(P_{10}C_9Si_1)_{1.1}$ alloys. It is speculated that the changes of strength and plasticity can be interpreted from the amorphicity and inclusions [30]. The achievement of yield point at high strength first manifests the absence of impurity inclusions which will lead to the unstable compressive deformation process and fracture before yield. The reduced plasticity also can be a proof for the high amorphicity and fewer clusters [31]. Fig. 8b and d show the SEM images of $Fe_{76}(P_{10}C_9Si_1)_{1.2}$ and $Fe_{78}(P_{10}C_9Si_1)_{1.1}$ amorphous rods after fracture. Two distinct fracture morphologies were found: shell-like pattern correlated with the bursting during fracture and vein-like pattern [32]. As enlarged in

Fig. 8c and e, the ratio of the typical vein-like patterns corresponding to the plastic deformation is higher for the $Fe_{76}(P_{10}C_9Si_1)_{1.2}$ alloy.

4. Discussion

Based on the former studies, $Fe_x(P_{10}C_9Si_1)_{5-0.05x}$ ($x = 76$–82) amorphous alloys with high AFA, excellent manufacturability and magnetic properties were successfully prepared with the pretreated molten iron from a blast furnace. The high AFA in large Fe content range, high impurity tolerance which can be prepared with IRMs and the new process should be interesting for the future development and commercialization. Since the melting process for master alloys, melt-spinning process for ribbons and mold casting processes for rod samples are all commonly used for amorphous alloys production which are proved to bring negligible composition difference, the composition difference of the amorphous products and the designed ones is neglectable. The underlying mechanisms will be discussed as follows.

First, it is unexpectedly that the $Fe_x(P_{10}C_9Si_1)_{5-0.05x}$ ($x = 76$–82) alloys exhibit superior impurity tolerance and can be made into rod and ribbon samples with low purity IRMs. The reasons are speculated in three aspects. 1) Although the pretreated molten iron from a blast furnace does contain a high content of impurity elements, the molten iron is in chemical equilibrium state and impurity elements are all dissolved. In other words, the molten iron can be thought of as a high purity prealloy with C, P, Si, Mn and Ti addition. As been well studied, the addition of Si, Mn and Ti can improve the AFA in many alloy
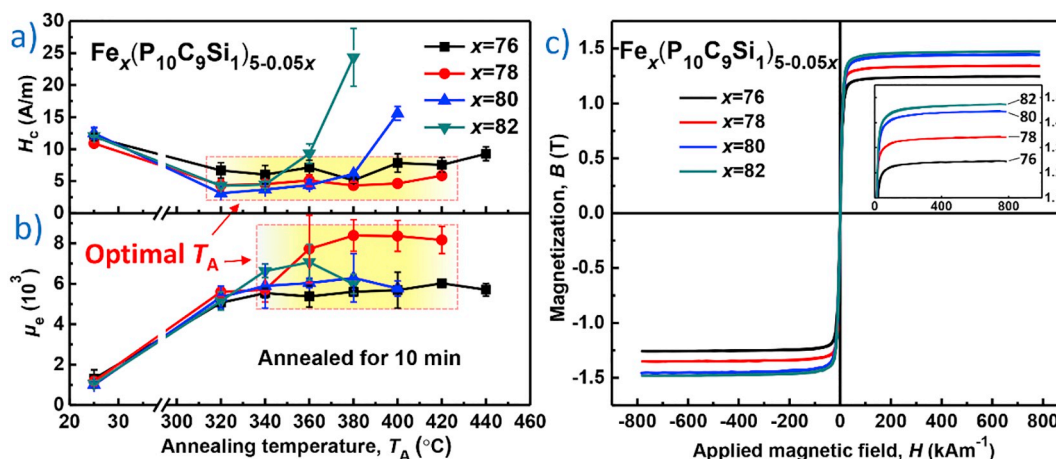

Fig. 6. a-b) T_A dependence of H_c and μ_e at 1 kHz for IRMs $Fe_x(P_{10}C_9Si_1)_{5-0.05x}$ ($x = 76, 78, 80, 82$) alloys ribbon annealed for 10 min; b) saturated magnetization loops of optimally annealed samples.

Table 2
The critical diameters, thermal parameters, magnetic properties and oxygen content of $Fe_x(P_{10}C_9Si_1)_{5-0.05x}$ (x = 76, 78, 80, 82) alloys prepared with IRMs.

Alloys	d_{max} (mm)	Thermal properties						Magnetic properties			O content (wppm)
		T_c (°C)	T_g (°C)	T_{x1} (°C)	T_m (°C)	T_{lm} (°C)	T_{ls} (°C)	B_s (T)	H_c (A/m)	μ_e ($\times 10^3$)	
$Fe_{76}P_{12}C_{10.8}Si_{1.2}$	1.5	295	446	475	951	1031	948	1.25	5.1	6.1	14
$Fe_{78}P_{11}C_{9.9}Si_{1.1}$	1.5	302	429	462	952	1030	944	1.35	4.3	8.4	18
$Fe_{80}P_{10}C_9Si_1$	1.5(air)	303	/	434	952	1025	969	1.45	3.1	6.3	16
$Fe_{82}P_9C_{8.1}Si_{0.9}$	< 1	301	/	422	948	1024	940	1.48	4.2	7.0	18

systems. 2) The P and Si are also commonly used in alloying steel industry, which have high solubility in molten iron. For $Fe_x(P_{10}C_9Si_1)_{5-0.05x}$ (x = 76–82) alloys, the addition of P and Si will not substantially change the balance of the molten and will not lead to the formation of refractory compounds which act as inclusions of impurities [21]. 3) The $Fe_x(P_{10}C_9Si_1)_{5-0.05x}$ (x = 76–82) alloys are selected and adjusted according to the novel processes in Fig. 1, the impurities containing C, P and Si in the molten iron from a blast furnace were used as useful components, while other minor impurities like Ti and Mn do not apparently affect the GFA and magnetic properties.

Second, we would like to unveil the high AFA of the $Fe_x(P_{10}C_9Si_1)_{5-0.05x}$ (x = 76–82) alloys. As the first reported Fe-based amorphous alloys with excellent magnetic properties, the base $Fe_{80}P_{10}C_9$ alloy is near-deep-eutectic composition and meet the amorphous forming rules including mixed enthalpy, atom size mismatch [3]. In this study, the minor addition of Si and adjustment of Fe content further decrease the T_m and T_{ls} which make the compositions closer to the deep-eutectic point. The increase of Fe content although reduces the intensity of glass transition, but does not decrease the crystallization temperature apparently, mitigating the side effect on AFA of the $Fe_x(P_{10}C_9Si_1)_{5-0.05x}$ (x = 76–82) alloys. In addition, the Si content was adjusted to the optimal value and the compositions were adapted to the industrial raw materials and process.

Last, we want to discuss the advantages of the novel processes and the magnetic properties of the alloys. According to the comparative study, calculation and test results, we can draw a rough comprehensive comparison shown in Fig. 9. Since the Fe-P pre-alloy is commonly used in iron industrial and very cheap (listed in Table 1), the $Fe_x(P_{10}C_9Si_1)_{5-0.05x}$ (x = 76–82) alloys based on molten iron exhibit lower cost than Si-steel. Compared with the commercial FeSiB amorphous alloy and FeSiBNbCu nanocrystalline alloys, the cost of raw materials is reduced to about 40% and 10%, respectively, as shown in Fig. 9a. Compared with the Si-steel production process with complicated purification, alloying, annealing, rolling, and orientation sub-

processes in a production line which is always 1–2 km long, the novel process proposed in Fig. 1 is much more energy efficient. The residual heat in molten iron can be subsequently used in the pretreatment, alloying and melt-spinning processes. At a conservative estimate, the energy consumption of this novel process is only about 10% of the Si-steel, 40% of the commercial FeSiB amorphous alloy and 30% of the FeSiBNbCu nanocrystalline alloys. For the magnetic properties, the B_s of the FePCSi alloys is lower than Si-steel and FeSiB amorphous alloy, but higher than FeSiBNbCu nanocrystalline alloys. The H_c of the FePCSi alloys is comparative with the FeSiB amorphous alloy and much lower than the Si-steel [33]. Overall, the novel process based on pretreated molten iron from a blast furnace exhibits attractive advantages including energy-efficient and short process. The FePCSi amorphous alloys have the superiority of ultra-low cost of raw materials, outstanding magnetic properties and good manufacturability.

5. Conclusion

In this study, a novel ultra-low cost and energy-efficient production process based on pretreated molten iron was proposed and the $Fe_x(P_{10}C_9Si_1)_{5-0.05x}$ (x = 76–82) amorphous alloys were successfully developed. Compare to the alloys prepared with PRMs, the FePCSi alloys prepared with IRMs exhibit high impurity tolerance and manufacturability. The main results are as follows:

1) The $Fe_x(P_{10}C_9Si_1)_{5-0.05x}$ (x = 76, 78, 80, 82) amorphous alloys prepared with pretreated molten iron exhibit superb impurity tolerance and manufacturability. The alloys can be cast into rod samples with critical dimensions up to 1.5 mm and melt-spun into ribbons with high ductility as well as excellent surface quality.
2) The optimally annealed ribbons exhibit high magnetic performance, containing low H_c of 3.1–5.1 A/m, high μ_e of 6.1–8.4 $\times 10^3$ at 1 kHz, and high B_s of 1.25–1.48 T. The as-cast rods exhibit high compressive fracture strength of 3.25–3.37 GPa.
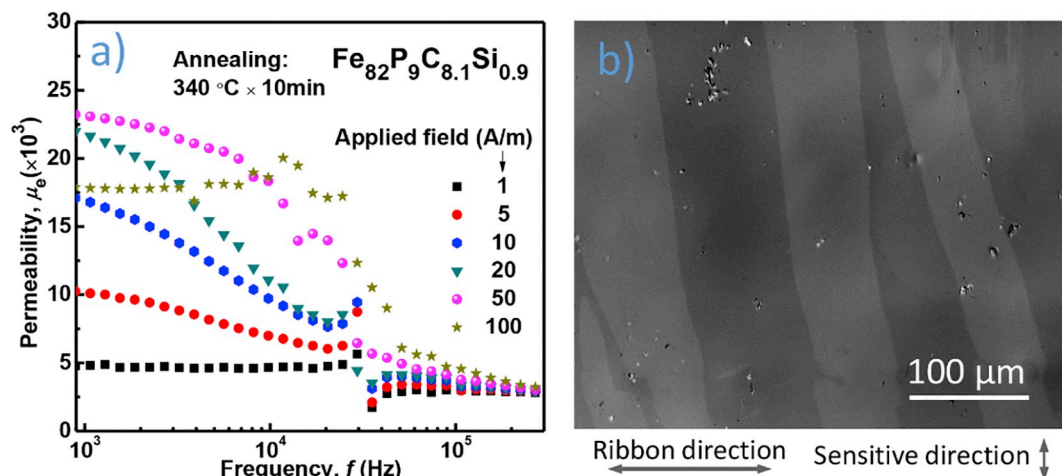

Fig. 7. IRMs $Fe_{82}(P_{10}C_9Si_1)_{0.9}$ amorphous ribbons annealed at 340 °C for 10 min, a) Frequency dependence of μ_e measured under different AC magnetic field amplitude; b) magnetic domains of ribbon samples.
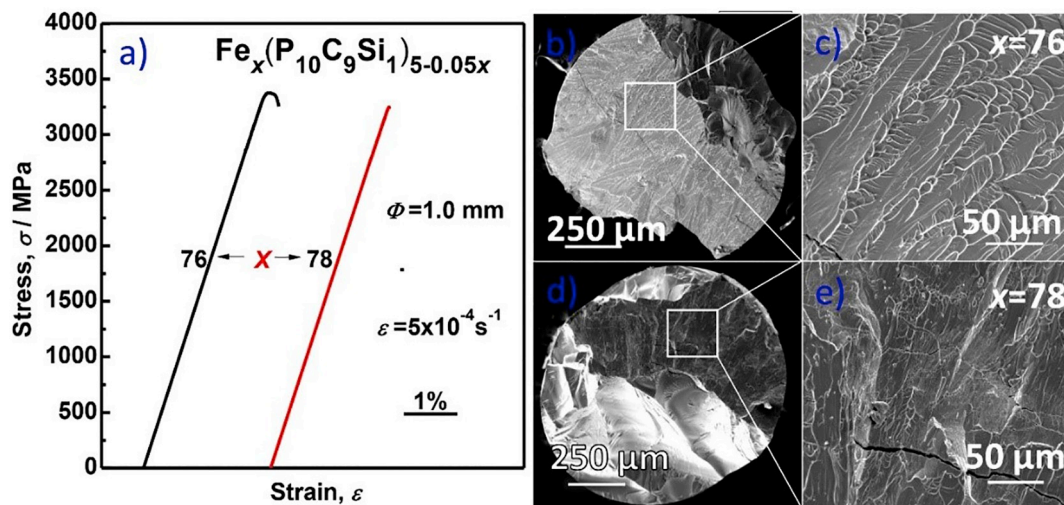
Fig. 8. a) Compressive stress-strain curves of $Fe_x(P_{10}C_9Si_1)_{5-0.05x}$ (*x* = 76, 78) amorphous rods prepared with IRMs; b-e) SEM images of fracture surface after compression tests.
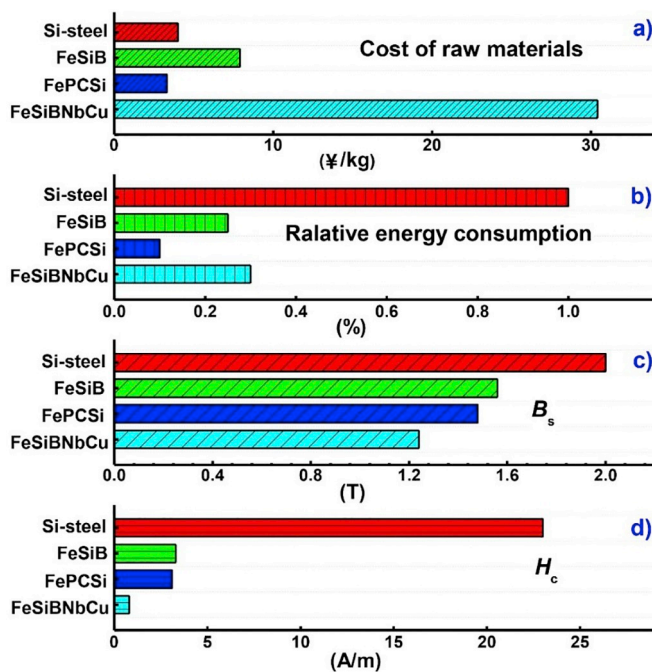

Fig. 9. Comprehensive comparisons of the current $Fe_x(P_{10}C_9Si_1)_{5-0.05x}$ alloys with the typical commercial soft-magnetic materials.

3) The novel production process for Fe-based amorphous alloys based on the pretreated molten iron from a blast furnace can well use the impurity elements like C, P, and Si as useful components. The dissolved elements of Mn, Ti and other elements in the raw materials do not apparently affect the AFA and properties of the alloys adopted to the process. The cost of raw materials is reduced to about 40% of the FeSiB alloy and 10% of the FeSiBNbCu alloy.

4) The new production process of FePCSi amorphous alloys can use the residual heat in molten iron in the alloying and melt-spinning processes. The energy consumption of this process is only about 10% of the Si-steel, 40% of the FeSiB alloy and 30% of the FeSiBNbCu alloy.

Acknowledgements

References

[1] M.E. McHenry, M.A. Willard, D.E. Laughlin, Amorphous and nanocrystalline materials for applications as soft magnets, Prog. Mater. Sci. 44 (1999) 291–433.
[2] A. Wang, C. Zhao, A. He, H. Men, C. Chang, X. Wang, Composition design of high B-s Fe-based amorphous alloys with good amorphous-forming ability, J. Alloys Compd. 656 (2016) 729–734.
[3] J.F. Wang, R. Li, N.B. Hua, L. Huang, T. Zhang, Ternary Fe-P-C bulk metallic glass with good soft-magnetic and mechanical properties, Scr. Mater. 65 (2011) 536–539.
[4] A. Makino, T. Kubota, M. Makabe, C.T. Chang, A. Inoue, FeSiBP metallic glasses with high glass-forming ability and excellent magnetic properties, Mater. Sci. Eng. B Adv. 148 (2008) 166–170.
[5] F.J. Liu, K.F. Yao, H.Y. Ding, Fe-based glassy alloys with high iron content and high saturation magnetization, Intermetallics 19 (2011) 1674–1677.
[6] C. Suryanarayana, A. Inoue, Iron-based bulk metallic glasses, Int. Mater. Rev. 58 (2013) 131–166.
[7] J.C. Qiao, Y. Yao, J.M. Pelletier, L.M. Keer, Understanding of micro-alloying on plasticity in Cu46Zr47-xAl7Dyx (0 ≤ x ≤ 8) bulk metallic glasses under compression: based on mechanical relaxations and theoretical analysis, Int. J. Plast. 82 (2016) 62–75.
[8] Y. Cai, H. Ling, T. Jiang, Effect of industrial raw materials on the glass-forming ability, magnetic and mechanical properties of Fe-based bulk metallic glasses, Metall. Mater. Trans. B Process Metall. Mater. Process. Sci. 46 (2015) 2484–2489.
[9] H.X. Li, J.E. Gao, S.L. Wang, S. Yi, Z.P. Lu, Formation, crystallization behavior, and soft magnetic properties of FeCSiBP bulk metallic glass fabricated using industrial raw materials, Metall. Mater. Trans. A 43A (2012) 2615–2619.
[10] N. Morito, Effect of carbon on surface crystallization of amorphous Fe-B-Si alloy induced by selective oxidation, Mat. Sci. Eng. A Struct. 129 (1990) 119–125.
[11] H.W. Kui, A.L. Greer, D. Turnbull, Formation of bulk metallic-glass by fluxing, Appl. Phys. Lett. 45 (1984) 615–616.
[12] D. Granata, E. Fischer, V. Wessels, J.F. Loffler, Fluxing of Pd-Si-Cu bulk metallic glass and the role of cooling rate and purification, Acta Mater. 71 (2014) 145–152.
[13] A. Inoue, B.L. Shen, H. Koshiba, H. Kato, A.R. Yavari, Cobalt-based bulk glassy alloy with ultrahigh strength and soft magnetic properties, Nat. Mater. 2 (2003) 661–663.
[14] A. Inoue, B.L. Shen, A new Fe-based bulk glassy alloy with outstanding mechanical properties, Adv. Mater. 16 (2004) 2189–2192.
[15] L. Xie, T. Liu, A.N. He, Q. Li, Z.K. Gao, A.D. Wang, C.T. Chang, X.M. Wang, C.T. Liu, High B (s) Fe-based nanocrystalline alloy with high impurity tolerance, J. Mater. Sci. 53 (2018) 1437–1446.
[16] J. Pang, A.D. Wang, S.Q. Yue, F.Y. Kong, K.Q. Qiu, C.T. Chang, X.M. Wang, C.T. Liu, Fluxing purification and its effect on magnetic properties of high-B-s FeBPSiC amorphous alloy, J. Magn. Magn. Mater. 433 (2017) 35–41.
[17] A. Wang, C. Zhao, H. Men, A. He, C. Chang, X. Wang, R.-W. Li, Fe-based amorphous alloys for wide ribbon production with high B-s and outstanding amorphous forming ability, J. Alloys Compd. 630 (2015) 209–213.
[18] T. Zhang, F. Liu, S. Pang, R. Li, Ductile Fe-based bulk metallic glass with good soft-magnetic properties, Mater. Trans. 48 (2007) 1157–1160.
[19] A. Inoue, B. Shen, Soft magnetic bulk glassy Fe-B-Si-Nb alloys with high saturation magnetization above 1.5 T, Mater. Trans. 43 (2002) 766–769.
[20] S. Lee, H. Kato, T. Kubota, K. Yubuta, A. Makino, A. Inoue, Excellent thermal stability and bulk glass forming ability of Fe-B-Nb-Y soft magnetic metallic glass,

Mater. Trans. 49 (2008) 506–512.

[21] J.S. Yu, Y.Q. Zeng, T. Fujita, T. Hashizume, A. Inoue, T. Sakurai, M.W. Chen, On the effect of impurities in metallic glass formation, Appl. Phys. Lett. 96 (2010) 3.

[22] A. Inoue, Stabilization of metallic supercooled liquid and bulk amorphous alloys, Acta Mater. 48 (2000) 279–306.

[23] C.T. Chang, J.H. Zhang, B.L. Shen, W.H. Wang, A. Inoue, Pronounced enhancement of glass-forming ability of Fe-Si-B-P bulk metallic glass in oxygen atmosphere, J. Mater. Res. 29 (2014) 1217–1222.

[24] S. Yue, H. Zhang, R. Cheng, A. Wang, Y. Dong, A. He, H. Ni, C.-T. Liu, Magnetic and thermal stabilities of FeSiB eutectic amorphous alloys: compositional effects, J. Alloys Compd. 776 (2019) 833–838.

[25] X. Liang, A. He, A. Wang, J. Pang, C. Wang, C. Chang, K. Qiu, X. Wang, C.-T. Liu, Fe content dependence of magnetic properties and bending ductility of FeSiBPC amorphous alloy ribbons, J. Alloys Compd. 694 (2017) 1260–1264.

[26] C.L. Zhao, A.D. Wang, A.N. He, S.Q. Yue, C.T. Chang, X.M. Wang, R.W. Li, Correlation between soft-magnetic properties and T-x1-T-c in high B-s FeCoSiBPC amorphous alloys, J. Alloys Compd. 659 (2016) 193–197.

[27] Z.P. Lu, C.T. Liu, Glass formation criterion for various glass-forming systems, Phys.

Rev. Lett. 91 (2003) (115505–115501).

[28] C. Wang, A. He, A. Wang, J. Pang, X. Liang, Q. Li, C. Chang, K. Qiu, X. Wang, Effect of P on glass forming ability, magnetic properties and oxidation behavior of FeSiBP amorphous alloys, Intermetallics 84 (2017) 142–147.

[29] H. Matsumoto, A. Urata, Y. Yamada, A. Inoue, FePBNbCr soft-magnetic glassy alloys with low loss characteristics for inductor cores, J. Alloys Compd. 504 (2010) S139–S141.

[30] A.S. Nouri, X.J. Gu, S.J. Poon, G.J. Shiflet, J.J. Lewandowski, Chemistry (intrinsic) and inclusion (extrinsic) effects on the toughness and Weibull modulus of Fe-based bulk metallic glasses, Philos. Mag. Lett. 88 (2008) 853–861.

[31] B.A. Sun, W.H. Wang, The fracture of bulk metallic glasses, Prog. Mater. Sci. 74 (2015) 211–307.

[32] Z.F. Zhang, G. He, J. Eckert, L. Schultz, Fracture mechanisms in bulk metallic glassy materials, Phys. Rev. Lett. 91 (2003).

[33] O. Gutfleisch, M.A. Willard, E. Brück, C.H. Chen, S.G. Sankar, J.P. Liu, Magnetic materials and devices for the 21st century: stronger, lighter, and more energy efficient, Adv. Mater. 23 (2011) 821–842.